6 High-Resolution Numerical Models for Smoke Transport in Plumes from Wildland Fires

Philip Cunningham
Earth and Environmental Sciences Division, Los Alamos National Laboratory
Los Alamos, New Mexico 87545, USA
Email: pcunning@lanl.gov

Scott L. Goodrick
Center for Forest Disturbance Science, US Forest Service
Athens, Georgia 30602, USA
Email: sgoodrick@fs.fed.us

Abstract A high-resolution large-eddy simulation (LES) model is employed to examine the fundamental structure and dynamics of buoyant plumes arising from heat sources representative of wildland fires. Herein we describe several aspects of the mean properties of the simulated plumes. Mean plume trajectories are apparently well described by the traditional two-thirds law for plume rise; however, the spatial structure of the mean plume is significantly different from the Gaussian distributions typically assumed in simple plume models. This discrepancy arises from the fact that entrainment properties of a buoyant plume in a cross wind are significantly different from those of a buoyant plume in the absence of a cross wind, a result of the interaction of the buoyancy-generated vorticity in the plume with the vorticity in the ambient wind. The depth of the crosswind shear layer at the surface also appears to play a role in both the horizontal and vertical spread of the plume boundaries downwind, and in particular the increase in horizontal spread acts to increase the departure from a Gaussian distribution seen in the plume cross sections.

Keywords Fire plumes, large-eddy simulations, smoke transport, plume rise, turbulent kinetic energy, vorticity and entrainment

6.1 Introduction

Predicting the impacts on air quality due to the smoke from prescribed fires and wildfires represents a central problem in smoke management, particularly for many locations in the Eastern United States where wildfire-prone regions are often located

near populated areas. A variety of models and tools are available for the purpose of modeling smoke impacts from wildland fires, and in many cases these models are appropriate and provide valuable information. These tools typically fall into three categories: simple Gaussian plume models, Lagrangian puff models, and Eulerian grid models.

Gaussian plume models, such as VSmoke (Lavdas, 1996) are frequently used by land managers during the planning phase of a prescribed burn. VSmoke assumes Gaussian dispersion in both the horizontal and vertical directions from a straight-line trajectory for each independent period of the simulation. VSmoke is designed to provide the best estimate of maximum concentrations of smoke at the surface, rather than accurate concentrations of smoke within the plume. To achieve this estimate, VSmoke allows the user to partition emissions between a component subject to plume rise, following the formulation of Briggs (1975), and a surface component that lacks the buoyancy to achieve significant rise.

As computing power has increased, the use of more complex descriptions of plume behavior, such as Lagrangian puff models, has become more widespread. Lagrangian puff models operate by releasing a series of puffs that are transported by spatially and temporally varying weather conditions. While within-puff dispersion is still handled in a Gaussian manner, puffs are allowed to split when subject to high levels of vertical wind shear. CALPUFF (Scire et al., 2000) is a Lagrangian puff model that is an integral component of the BlueSky smoke modeling framework (Ferguson, 2003). Plume rise from area sources in CALPUFF follows the derivation of Weil (1988), with the exception that the Boussinesq approximation employed by Weil (1988) is not made. CALPUFF assumes that the plumes will have a circular cross section despite evidence that fire plumes are often dominated by a pair of counter-rotating vortices; however, this may be an acceptable approximation since the presence of the counter-rotating vortices does not appear to impact plume rise calculations (Zhang, 1993; Zhang and Ghoniem, 1993).

Eulerian grid models are frequently used in air quality modeling for assessing the cumulative impact of a wide variety of emission sources at a regional scale and can include complex chemical transformations. Although the scale of these models is generally much larger than the scale of a wildland fire plume, air quality models such as the United States environmental protection agency (EPA) community multiscale air quality (CMAQ) modeling system (Byun and Ching, 1999) can contain subgrid-scale parameterizations for representing smaller scale features such as plumes from individual sources. In CMAQ this is handled by the plume-in-grid (PinG) formulation (Gillani and Godowitch, 1999), which behaves in the manner of a hybrid of the Gaussian and puff models. Transport is handled by the mean wind throughout the depth of the plume, similar to the use of a layer-mean wind in the Gaussian models. The plume itself is constructed as a succession of slabs perpendicular to the flow. The lateral spread of these slabs is governed by turbulence, wind shear and a background entrainment value, while the vertical spread of the plume is governed predominantly by turbulence. Each crossflow

slab is divided into a series of columns with an initially Gaussian lateral distribution of pollutants. After initialization, the lateral distribution of concentration is controlled by a series of mass balance equations, transferring concentration between columns through parameterized diffusion and entrainment processes.

Although these models have been applied with general success over a wide range of atmospheric conditions, they are all based on simplifications to the governing equations, and none of them is able to represent accurately the 3D turbulent dynamics of the plume itself and its interaction with the ambient atmosphere. It is of particular interest, then, to explore the fundamental dynamics of buoyant plumes arising from intense heat sources (e.g., plume trajectory, lateral and vertical spread, entrainment) to assess the utility and accuracy of the models currently in use for air quality assessment, and in particular to identify situations in which these models may have significant errors.

In a recent study, Cunningham et al. (2005) employed a high-resolution LES model to explore the dynamics of buoyant plumes arising from a heat source representative of wildland fires. This model was designed to resolve the majority of the turbulent eddies in the plume and its environment, and thus does not suffer from the approximations inherent to the models discussed above. The simulations shown by Cunningham et al. (2005) suggest that, even for simple configurations, plume behavior is highly complex and dominated by a variety of coherent vortex structures that may have a significant impact on smoke transport. In the present chapter, we continue and extend this investigation of the fundamental dynamics of buoyant plumes in a cross wind by describing the mean properties of the simulated plumes for different heat source intensities and different ambient wind conditions.

In the following section, the details of the numerical model are described briefly. In Section 6.3, the basic time-averaged properties of the simulated plumes and their dependence on the heat source strength and the ambient wind are shown, while Section 6.4 presents a summary of these results and directions for future research.

6.2 Numerical Model

For this study we utilize the LES model described by Cunningham et al. (2005). The governing equations are those for 3D, compressible flow in a density-stratified atmosphere forced by a prescribed volumetric heat source, Q:

$$\frac{\partial}{\partial t}(\rho u_i) + \frac{\partial}{\partial x_j}(\rho u_i u_j) + \frac{\partial p'}{\partial x_i} + g\rho'\delta_{i3} = \frac{\partial \tau_{ij}}{\partial x_j} - D_i \tag{6.1}$$

$$\frac{\partial}{\partial t}(\rho\theta) + \frac{\partial}{\partial x_j}(\rho\theta u_j) = \frac{\partial H_j}{\partial x_j} + \frac{Q\theta}{c_p T} \tag{6.2}$$

$$\frac{\partial \rho}{\partial t} + \frac{\partial}{\partial x_j}(\rho u_j) = 0 \tag{6.3}$$

where ρ is the density, u_i is the wind velocity in the x_i direction with $i, j, k =$ 1, 2, or 3 representing streamwise (x), spanwise (y), or vertical (z) directions, respectively, p' and ρ' are the departures of pressure and density, respectively, from a hydrostatic base state, D_i is a drag term intended to represent the effects of a vegetation canopy, T and θ are the temperature and potential temperature, and c_p is the specific heat at constant pressure.

A conventional approach to subgrid-scale modeling (e.g., Deardorff, 1973; Moeng and Wyngaard, 1988) is employed for the LES model, in which the subgrid-scale stress tensor, τ_{ij}, and the subgrid-scale heat flux, H_j, are represented respectively by

$$\tau_{ij} = \rho K_m \left(\frac{\partial u_i}{\partial x_j} + \frac{\partial u_j}{\partial x_i} \right) - \frac{2}{3} \rho K_m \frac{\partial u_k}{\partial x_k} \delta_{ij} \tag{6.4}$$

and

$$H_j = \rho K_h \frac{\partial \theta}{\partial x_j} \tag{6.5}$$

where K_m is the eddy viscosity and K_h is the eddy diffusivity.

The eddy viscosity is taken to depend on the subgrid-scale turbulent kinetic energy (TKE), e, as follows

$$K_m = C_k e^{1/2} \Delta \tag{6.6}$$

where C_k is a constant and Δ is the grid spacing. The eddy diffusivity is then related to the eddy viscosity via a turbulent Prandtl number, $Pr = K_m / K_h$, which is assumed to be equal to 1/3 herein. An additional equation for the subgrid-scale TKE is then required, and is given by

$$\frac{\partial}{\partial t}(\rho e) + \frac{\partial}{\partial x_j}(\rho e u_j) = -\tau_{ij} \frac{\partial u_i}{\partial x_j} + 2 \frac{\partial}{\partial x_j} \left(\rho K_m \frac{\partial e}{\partial x_j} \right) - \frac{\rho g K_h}{\theta} \frac{\partial \theta}{\partial z} - \frac{\rho C_e e^{3/2}}{\Delta} \tag{6.7}$$

where the last term on the right hand side represents the dissipation of subgrid-scale TKE. Following Moeng and Wyngaard (1988), values for the constants in Eq. (6.6) and Eq. (6.7) are chosen to be $C_k = 0.1$ and $C_e = 0.93$.

The heat source, Q, in Eq. (6.2) is intended to represent in an idealized manner the heating due to a fire of moderate intensity, and has the form of a smoothed top-hat distribution, as given by Eq. (6.10) in Cunningham et al. (2005). The heat source is centered at point (x_h, y_h), which is (450 m, 600 m) from the origin. The total heat release rate (HRR) is given by the volume integral of Q, and is taken to be constant after a ramp-up period of 10 s at the beginning of each simulation.

The governing equations are solved using the dynamical core of the weather research and forecasting (WRF) model (Skamarock et al., 2001). The computational domain is a rectangular box with spatial dimensions of 1,800 m in the streamwise direction (x), 1,200 m in the spanwise direction (y), and 1,800 m in the vertical direction (z). A uniform grid spacing of 10 m is employed in all directions. The ambient potential temperature is taken to be uniform and equal to 300 K in all simulations. For additional details of the numerical solution procedure, refer to Cunningham et al. (2005).

In an effort to explore the dependence of plume dynamics on the intensity of the heat source and on the nature of the ambient wind, several simulations have been performed for different heat source intensities, and different ambient wind profiles specified by

$$U(z) = U_0 \tanh(z/z_0) \tag{6.8}$$

Parameters employed for each simulation described here, along with the identifying label for each case, are provided in Table 6.1.

Table 6.1 Parameters for the simulations

Case	Heat source (MW)	U_0 (m·s^{-1})	z_0 (m)
Q2U3H50	350	3	50
Q2U3H100	350	3	100
Q2U5H50	350	5	50
Q2U5H100	350	5	100
Q3U5H50	525	5	50
Q3U5H100	525	5	100

In an effort to explore further the dynamics of buoyant plumes in a crossflow, in Chapter we examine the basic structure of various mean properties of simulated plumes. To explore these mean properties, simulations were performed for each case for 20,000 time steps, with statistical properties evaluated over the last 10,000 steps. Herein we examine the mean plume trajectories for each case, the mean structure of temperature and wind, and the mean TKE.

6.3 Dynamical Properties of Simulated Plumes

Instantaneous snapshots of potential temperature, vorticity magnitude, and vertical component of vorticity from the simulation *Q2U5H100* are shown in Fig. 6.1, and illustrate the characteristic plume structure as well as the highly vortical nature of the flow. It is apparent from these images that even in such simple initial configurations, the plume is highly turbulent and dominated by coherent vortical structures. These structures include the counter-rotating vortex pair aligned with

the plume trajectory that may be associated with bifurcation of the plume, transverse shear-layer vortices on the upwind face of the plume, and vertically oriented wake vortices that form downwind of the heat source and that extend from beneath the bent over plume down to the surface. These vortical structures are described and discussed in more detail by Cunningham et al. (2005).

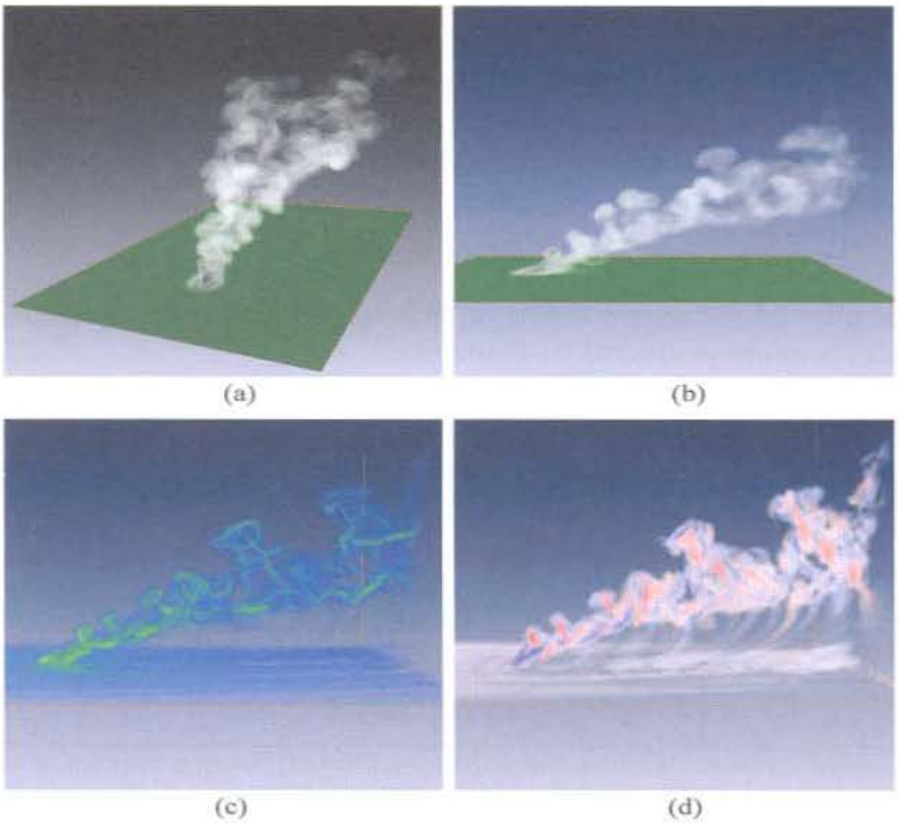

Figure 6.1 Instantaneous fields from the *Q2U5H*100 simulation. (a) and (b) Potential temperature from different view perspectives, (c) total vorticity magnitude, and (d) vertical component of vorticity (blue – positive values; red – negative values)

6.3.1 Mean Plume Trajectories

Mean plume trajectories for each case are depicted by the black and green lines in Fig. 6.2; these plume trajectories are calculated based on the maximum potential temperature deviation from ambient at each location downwind of the heat source along the plume centerline (i.e., the $x-z$ plane that intersects the center of the heat source). Also shown in Fig. 6.2 are trajectories predicted (based on heat source intensity and the magnitude of the ambient cross wind) by the traditional two-thirds law plume rise model of Briggs (1975) and its modification by Mills (1987) to account for finite-area sources.

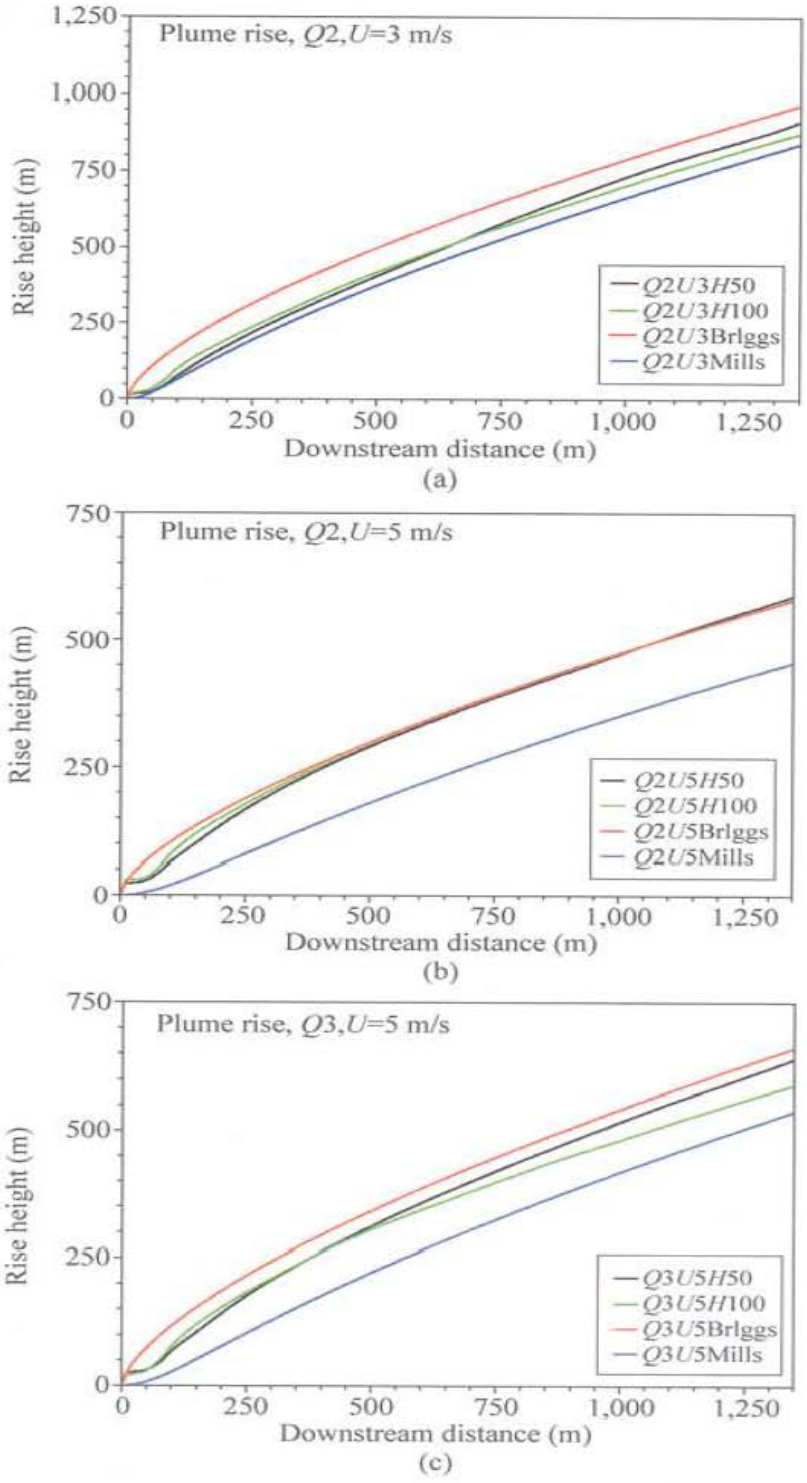

Figure 6.2 Simulated mean plume trajectories for (a) $Q2U3$ cases, (b) $Q2U5$ cases, and (c) $Q3U5$ cases. Trajectories for the shallow shear layer ($z_0 = 50$ m) are shown by black lines, while trajectories for the deeper shear layer ($z_0 = 100$ m) are shown by green lines. Also shown are plume rise calculations based on equations of Briggs (1975) and Mills (1987), depicted as red and blue lines, respectively

Following Briggs (1975), the rise height, h_B, for buoyancy-dominated plumes in a neutrally stratified atmosphere is given by

$$h_B = \left(\frac{3}{2\beta^2}\right)^{1/3} \frac{F_B^{1/3} x^{2/3}}{U_0} \tag{6.9}$$

where β is an empirically derived entrainment rate, typically chosen to have a value of 0.6, U_0 is the (constant) ambient wind speed, x is the distance downwind from the center of the source, and F_B is the buoyancy flux, given by

$$F_B = \frac{gQ_{tot}}{\pi \rho_a c_p T_a} \tag{6.10}$$

In Eq. (6.10), Q_{tot} is the total HRR, and ρ_a and T_a are an ambient air density and temperature, respectively. Trajectories calculated via Eq. (6.9) for a given heat source and ambient wind speed are shown by the red lines in Fig. 6.2.

Equation (6.9) assumes that the plume evolves from a point source, and it can be modified to account for a finite diameter, d, of the source (e.g., Mills, 1987; Zhang and Ghoniem, 1993), such that the plume rise height, h_M, is given by

$$h_M = \left(h_B^3 + \left(\frac{d}{2\beta}\right)^3\right)^{1/3} - \frac{d}{2\beta} \tag{6.11}$$

Trajectories calculated via Eq. (6.11) for a given heat source and ambient wind speed are shown by the blue lines in Fig. 6.2.

It is apparent that several fire diameters downstream of the heat source the mean plume rise seen in the simulations is well described by a power-law trajectory, and is in reasonably good agreement with the simple plume rise calculations. Nevertheless, the trajectories of the simulated plumes do exhibit some dependence on the depth of the shear layer in the ambient cross wind, as evidenced by the difference between the black and green lines. In particular, plume trajectories are slightly lower when the crosswind shear layer is deeper (e.g., Fig. 6.2(c)).

6.3.2 Mean Plume Structure

Despite the fact that the mean plume trajectories appear to be consistent with the well established two-thirds law for plume rise, the mean structure of the simulated plumes departs from the Gaussian or top-hat distribution often assumed in plume models. Indeed, as shown in Fig. 6.3, all of the simulated plumes exhibit a kidney-shaped, or even bifurcated, structure with a local minimum along the plume centerline resulting from the presence of the counter-rotating vortex pair.

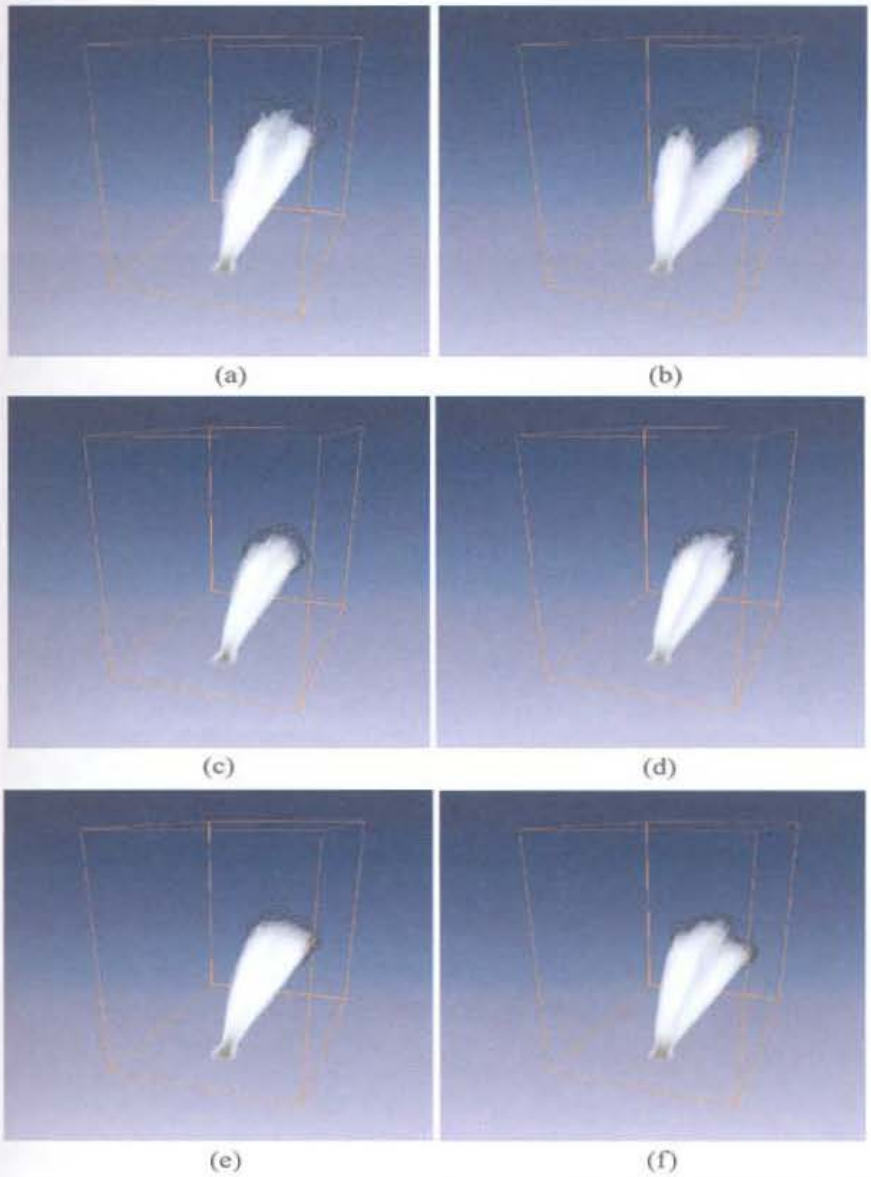

Figure 6.3 Mean potential temperature for case: (a) *Q2U3H*50, (b) *Q2U3H*100, (c) *Q2U5H*50, (d) *Q2U5H*100, (e) *Q3U5H*50, and (f) *Q3U5H*100

Figure 6.3 also illustrates the fact that the depth of the cross wind shear layer also has a significant impact on the mean structure of the plume, as discussed by Cunningham et al. (2005). Specifically, the lateral spread of the plume and the separation of the plume branches are greater for the deeper ambient shear layer. This property appears to result from the enhanced entrainment of ambient cross wind vorticity into the plume for the deeper shear layer, but this process requires further study and quantification.

Mean streamlines in the $y-z$ plane 1000 m downstream of the heat source are shown in Fig. 6.4; these streamlines illustrate clearly the presence of the counter-

rotating vortex pair in the time-averaged plume, and the associated upward vertical motion along the plume centerline. This upward motion may be important for PM transport, and may result in different downwind distributions for PM of different sizes (e.g., fine particles with smaller terminal velocities may be kept aloft along the centerline longer than larger particles).

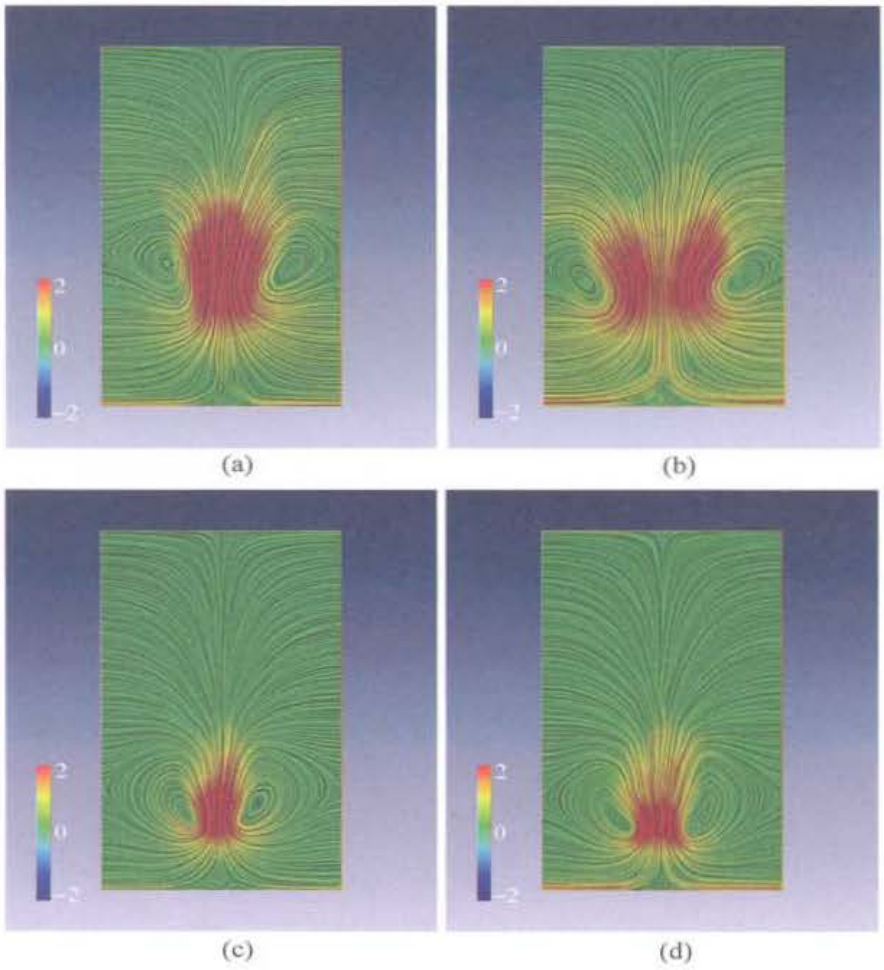

Figure 6.4 Mean streamlines in the $y-z$ plane at $x = 1{,}600$ m for case: (a) *Q2U3H50*, (b) *Q2U3H100*, (c) *Q2U5H50*, and (d) *Q2U5H100*. Color shading corresponds to vertical velocity in $m \cdot s^{-1}$

6.3.3 Turbulent Kinetic Energy (TKE)

Figure 6.5 shows mean subgrid and total (subgrid plus resolved) TKE for the *Q2U3H100* case, both in the $x-z$ plane along the plume centerline (Figs. 6.5(a) and (b)), and in the $y-z$ plane 1,000 m downstream of the heat source (Figs. 6.5(c) and (d)).

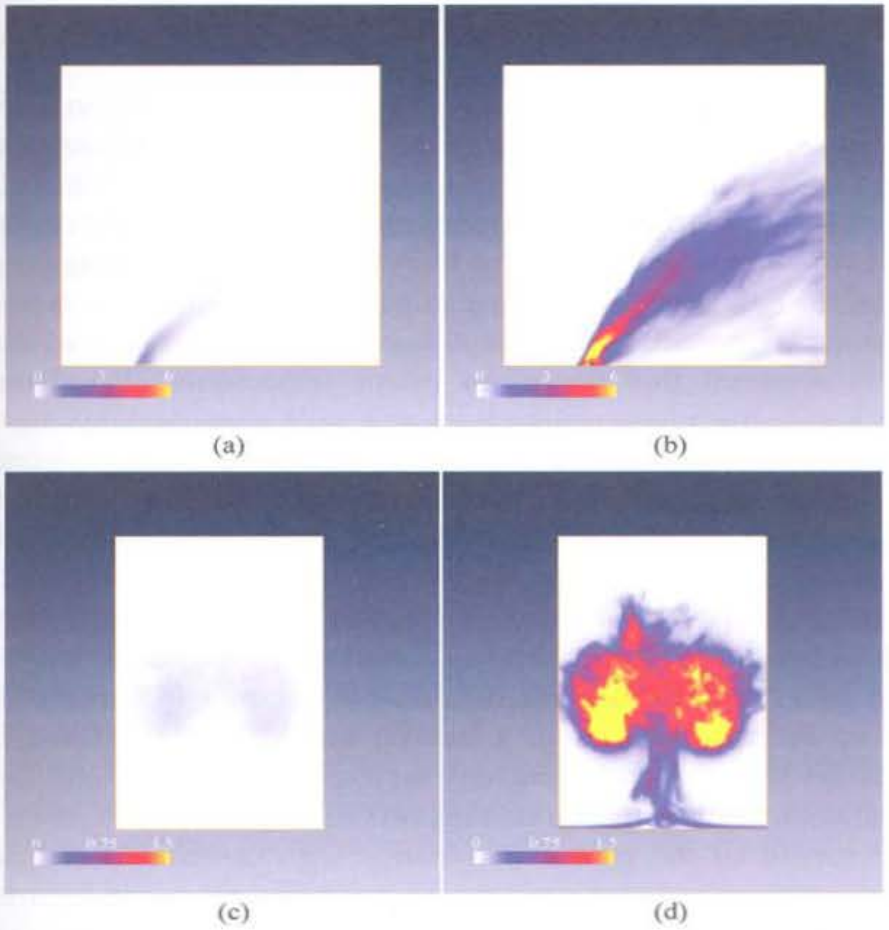

Figure 6.5 Mean turbulent kinetic energy ($m^2 \cdot s^{-2}$) for the $Q2U3H100$ case: (a) subgrid TKE along centerline, (b) total TKE along centerline, (c) subgrid TKE at $x = 1{,}600$ m, (d) total TKE at $x = 1{,}600$ m

First, it is apparent from these figures that the subgrid TKE is significantly smaller in magnitude than the total TKE, indicating that the energy containing eddies in the plume are well resolved on the grid employed in these simulations. Second, it is apparent that the turbulence seen in the simulations is dominated by the mean effect of the vortical structures seen in the instantaneous images. In particular, turbulence, and thus entrainment and mixing, along the centerline (Fig. 6.5(b)) is associated with the repeated passage of shear-layer vortices seen on the upwind face of the plume, whereas farther downwind the turbulence is dominated by the counter-rotating vortex pair (Fig. 6.5(d)).

It is of considerable interest to examine the dynamics of the transition between these turbulence regimes, and specifically how the distance downwind from the heat source at which this transition occurs depends on the parameters of the simulation, such as the intensity of the heat source and the depth of the crosswind shear layer. Investigation of this transition is part of future research.

6.4 Summary and Conclusions

Several simulations have been performed using a high-resolution LES model to examine the dynamics of buoyant plumes arising from heat sources representative of wildland fires. This model is capable of representing the 3D turbulent eddies characteristic of such plumes, and is being employed in an effort to understand the fundamental structure and dynamics of buoyant plumes, including the nature and importance of the coherent vortical structures that are common to these flows.

In this Chapter we describe several aspects of the mean properties of the simulated plumes. It is apparent that the mean plume trajectories (based on potential temperature along the plume centerline) are well described by the traditional two-thirds law for plume rise; however, the spatial structure of the mean plume is significantly different from the Gaussian distributions typically assumed in simple plume models. This discrepancy arises from the fact that entrainment properties of a buoyant plume in a cross wind are significantly different from those of a buoyant plume in the absence of a cross wind, a result of the interaction of the buoyancy-generated vorticity in the plume with the vorticity in the ambient wind.

While the two-thirds plume rise formulation appears to agree well with the simulations of buoyant plumes in a neutral atmosphere presented herein, the modeling results raise several questions for further investigation. The depth of the crosswind shear layer at the surface appears to play a role in both the horizontal and vertical spread of the plume boundaries with downwind distance, and in particular the increase in horizontal spread acts to increase the departure from a Gaussian distribution seen in the plume cross sections. Source strength, or fire intensity, as well as shear layer depth influence the vertical spread of the plume, with intense fires and deeper shear layers providing enhanced vertical plume spread. How well these plume spread results agree with those predicted by current plume formulations is an open area for research.

Ongoing and future research is focused on the continued analysis of these simulations in an attempt to: ① quantify further the nature of the turbulent entrainment in these plumes, and how the entrainment depends on the vortical structures seen in the simulations; and ② examine the nature of turbulent transport in the plume (e.g., of PM of a range of sizes).

Acknowledgements

This research was partially supported by the USDA Forest Service, via a cooperative agreement with the USDA Forest Service Southern Research Station, and by the FSU School of Computational Science, via a grant of resources on the IBM SP Series 690 Power4-based supercomputer "Eclipse".

References

Briggs GA, (1975), Plume rise predictions. In: Lectures on Air Pollution and Environmental Impact Analysis, Haugen DA (Ed.), American Meteorological Society: 59 – 111

Byun DW, Ching JKS, (1999), Science algorithms of the EPA Models-3 Community Multiscale Air Quality (CMAQ) Modeling System, EPA-600/R-99/030, U.S. Environmental Protection Agency, Research Triangle Park, NC

Cunningham P, Goodrick SL, Hussaini MY, Linn RR, (2005), Coherent vortical structures in numerical simulations of buoyant plumes from wildland fires, *Int. J. Wildland Fire*, **14**: 61 – 75

Deardorff JW, (1973), The use of subgrid transport equations in a three-dimensional model of atmospheric turbulence, *J. Fluids Eng.* **95**: 429 – 438

Ferguson SA, (2003), Real-time mesoscale model forecasts for fire and smoke management: Preprints, Fifth Symp. on Fire and Forest Meteorology, Orlando, FL, American Meteorological Society

Gillani NV, Godowitch JM, (1999), Plume-in-grid treatment of major point source emissions. In: Science algorithms of the EPA Models-3 Community Multiscale Air Quality (CMAQ) Modeling System, Byun DW and Ching JKS (Eds.), EPA-600/R-99/030, U.S. Environmental Protection Agency, 9-1 – 9-39

Lavdas LG, (1996), Program VSMOKE – Users Manual, General Technical Report SRS-6, USDA Forest Service, Southern Research Station

Mills MT, (1987), Modelling the release and dispersion of toxic combustion products from pool fires, Proceedings, Int. Conf. on Vapor Cloud Modeling, Cambridge, MA

Moeng C-H, Wyngaard JC, (1988), Spectral analysis of large-eddy simulations of the convective boundary layer, *J. Atmos. Sci.* (45): 3573 – 3587

Scire JS, Strimaitis DG, Yamartino RJ, (2000), A User's Guide for the CALPUFF Dispersion Model, Earth Tech, Inc., Concord, MA

Skamarock WC, Klemp JB, Dudhia J, (2001), Prototypes for the WRF (Weather Research and Forecasting) model, Preprints, Ninth Conf. on Mesoscale Processes, Fort Lauderdale, FL, American Meteorological Society, J11 – J15

Weil JC, (1988), Plume rise. In: Lectures on Air Pollution Modeling, Venkatram A and Wyngaard JC, (Eds.), American Meteorological Society: 119 – 166

Zhang X, (1993), A computational analysis for the rise, dispersion and deposition of buoyant plumes, Ph D. Thesis, Massachusetts Institute of Technology, Cambridge

Zhang X, Ghoniem AF, (1993), A computational model for the rise and dispersion of wind-blown, buoyancy-driven plumes—I. Neutrally stratified atmosphere, *Atmos. Env.* **15**: 2295 – 2311